Quantum phase transitions in $Ba_{(1-x)}Ca_xFe_{12}O_{19}$ ($0 \leqslant x \leqslant 0.10$)

Keshav Kumar and Dhananjai Pandey*

School of Materials Science and Technology, Indian Institute of Technology (Banaras Hindu University), Varanasi-221005, India

(Received 3 April 2017; published 10 July 2017)

The ground state of $BaFe_{12}O_{19}$ (BFO) is controversial as three different quantum states, namely, quantum paraelectric, frustrated antiferroelectric, and quantum electric dipole liquid (QEDL), have been proposed. We have investigated the quantum critical behavior of BFO as a function of chemical pressure (a nonthermal variable) generated by smaller isovalent ion Ca^{2+} at the Ba^{2+} site. Analysis of synchrotron x-ray diffraction data confirms that Ca^{2+} substitution generates positive chemical pressure. Our dielectric measurements reveal that Ca^{2+} substitution drives BFO away from its quantum critical point (QCP) and stabilizes a quantum electric dipolar glass state whose dielectric peak temperature (T_c) increases with increasing Ca^{2+} content as $T_c \sim (x-x_c)^{1/2}$, a canonical signature of quantum phase transitions. Our dielectric measurements reveal that pure BFO is slightly away from its QCP with a T_c of 2.91 K. Specific-heat measurements reveal excess specific heat of non-Debye and nonmagnetic origin with linear temperature dependence below T_c which could be due to the QEDL state of BFO.

DOI: 10.1103/PhysRevB.96.024102

I. INTRODUCTION

Classical phase transitions, like boiling of water, are ubiquitous in nature and affect our day-to-day life. They occur at finite transition temperatures (T_c) as a result of a competition between the energy of the low-temperature phase and the entropy fluctuations with an energy scale of k_BT. Quantum phase transitions (QPTs), on the other hand, occur at the quantum critical point (QCP) $T_c = 0$ K (absolute zero) as a result of the competition between the energy of the system and the quantum fluctuations of energy scale $\hbar\omega$, where ω is the zero-point vibrational frequency of quantum oscillator. Although the QCP ideally occurs at absolute zero temperature, which is not experimentally realizable, its remarkable impact on several exotic phenomena occurring at finite temperatures (e.g., high-temperature superconductivity, metal insulator transition, integer and fractional Hall effects) makes it an area of vigorous research in condensed matter and materials science [1–7]. The QCP has been located in a variety of strongly correlated [8–12] and other systems (KH_2PO_4) [13] by gradually tuning the T_c close to 0 K through nonthermal variables, such as composition (x), pressure (p), and electric (E) or magnetic (H) field [13–17]. The fingerprints of the QPT persist above the QCP also in the so-called "quantum critical" regime also where quantum fluctuations dominate over the thermal fluctuations (i.e., $\hbar\omega > k_BT$) and give rise, for example, to nonclassical exponents for the dependence of T_c on the nonthermal control parameters. Interestingly, Nature has provided us with a family of materials called quantum paraelectrics (QPE), such as $SrTiO_3$ [18], $KTaO_3$ [19], $CaTiO_3$ [20], TiO_2 [21], and $EuTiO_3$ [22], which already possess a QCP and one can study the effect of quantum fluctuations in the quantum critical regime by driving the system away from the QCP on application of nonthermal variables [16,23].

Very recently, in a series of publications [24,25] it has been argued that M-type hexaferrites, especially the $BaFe_{12}O_{19}$ (BFO), are also QPE. First-principles calculations on BFO have revealed one-dimensional chains of electric dipoles arranged on a triangular lattice with ferroelectric (FE) and antiferroelectric (AFE) interactions along the c axis and in the ab plane, respectively, arising out of two unstable Γ-point optical phonon modes [26]. On account of the AFE interactions between the neighboring dipoles on the triangular lattice, BFO is geometrically frustrated [26,27]. The concept of frustration in the field of ferroelectrics and relaxors is not new but the frustration in BFO is unique because of its geometrical nature. The previously reported frustrated systems were based on competing AFE and FE interactions [28–31]. The reports on quantum saturation of $\varepsilon'(T)$ in BFO below $T \sim 10$ K (a canonical signature for the quantum paraelectricity) have become questionable because of the observation of an upturn in the $1/\varepsilon'(T)$ versus T plot around 4 K with a $1/T^3$-like dependence of $\varepsilon'(T)$ in agreement with the theory of uniaxial quantum paraelectrics [32]. First-principles density functional theory calculations in conjunction with Monte Carlo simulations using a simple dipole-dipole interaction model also suggest the possibility of a phase transition at $T_c \sim 3$ K to a geometrically frustrated AFE state [26]. The complex interplay of geometrical frustration and quantum fluctuations in BFO offers tremendous potential for the discovery of new exotic states of matter with phenomenological similarities with their magnetic counterparts [2,5,33–36] notwithstanding the intrinsic differences in the microscopic origin and dynamics of electrical and magnetic dipoles [27]. In fact, it has already been proposed that the exotic quantum spin-liquid-like state involving electric dipoles may exist in BFO at very low temperatures [27].

In the present work, we have investigated the effect of a nonthermal variable, namely, chemical pressure and local electric field, generated through substitution of Ba^{2+} ($r = 1.49$ Å) with a much smaller isovalent ion Ca^{2+} ($r = 0.99$ Å), on the quantum critical behavior of BFO using dielectric and specific-heat measurements from 1.66 to 100 K and 1.8 to 300 K, respectively. We observe a cusp in the dielectric permittivity of BFO at $T_c \sim 2.91$ K with negative Curie-Weiss (T_{CW}) temperature expected for AFE correlations, in excellent agreement with the theoretical predictions [26]. By analyzing the

*Corresponding author: dp.mst1979@gmail.com

specific-heat data with and without magnetic field, we have found evidence for excess specific heat of non-Debye and nonmagnetic origin which is approximately linear in T below $T_c = 2.91$ K supporting the possibility of a quantum electric dipole liquid (QEDL) state at low temperatures in agreement with the earlier report based on thermal conductivity measurements [27]. The T_c of BFO is shown to increase with increasing Ca^{2+} content (x) in the $(x-x_c)^{1/2}$ manner, characteristic of phase transitions in the quantum critical regime [16,37–39] in marked contrast to the $T_c \sim (x-x_c)$ type dependence expected for the classical regime [16,39]. Our dielectric results reveal that $Ba_{(1-x)}Ca_xFe_{12}O_{19}$ (BCFO-x) does not exhibit long range ordered AFE ground state, but may correspond to a QEDL-like state for pure BFO ($x = 0$), and quantum electric dipole glass state with frustrated AFE interactions for higher Ca^{2+} content ($x > 0.03$).

II. EXPERIMENTAL DETAILS AND ANALYSIS

The barium hexaferrite ($BaFe_{12}O_{19}$) and Ca^{2+}-doped $BaFe_{12}O_{19}$ were synthesized by the solid-state thermochemical reaction route using analytical reagent grade chemicals: $BaCO_3$ ($\geqslant$99.0% assay, Sigma Aldrich), Fe_2O_3 ($\geqslant$99.0% assay, Sigma Aldrich), and $CaCO_3$ ($\geqslant$99.5% assay, Alfa Aesar). A stoichiometric mixture of chemicals was mixed properly using an agate mortar and pestle for 3 h followed by ball milling in zirconia jar and balls which acted as the grinding medium. Acetone was used as a milling medium. Mixing was done for 12 h. The sample was dried at room temperature after mixing. Calcinations were carried out in alumina crucibles. Pure $BaFe_{12}O_{19}$ was synthesized by calcination at 1100 °C for 6 h. The Ca^{2+}-doped samples were calcined at 1250 °C for 6 h. The calcined powders were further crushed using a mortar and pestle. Then a few drops of 2% polyvinyl alcohol (PVA) were added to it as a binder. Pellets were made using cylindrical steel die and a uniaxial hydraulic press machine. Pellets were kept at 600 °C for 10 h to remove the PVA. A pure $BaFe_{12}O_{19}$ sample was sintered at 1200 °C for 6 h, whereas the Ca^{2+}-doped samples were sintered at 1275 °C for 1 h.

Room-temperature synchrotron x-ray diffraction (SXRD) data were collected at a wavelength of 0.207150 Å at P02.1 beamline in Petra III, Hamburg, Germany. For the SXRD measurements, the powder used was obtained from sintered pellets which were crushed into fine powders and then annealed at 600 °C for 10 h to remove the stresses introduced during crushing. Rietveld refinement was carried out using FULLPROF SUITE [40].

For dielectric measurements, the top and bottom surfaces of the sintered pellets were mildly polished using diamond paste. After polishing, the pellets were kept in isopropyl alcohol to remove moisture and then electroded using fired-on (500 °C for 2 min) silver paste. Low-temperature dielectric permittivity of $BaFe_{12}O_{19}$ was measured for all the samples using a fully computer controlled measuring system involving a Novocontrol Alpha-A High Frequency Analyzer and a cryogen free measurement system. First the measurements were carried out in the range 1.66–100 K at a heating rate of 0.3 K per minute at a fixed frequency of 300 kHz. This was followed by dielectric measurements over the temperature range 1.66–25 K at multiple frequencies in the range 10–400 kHz.

For heat-capacity measurements, a small piece of sintered pellet was used after annealing at 600 °C for 10 h. The heat-capacity measurement of pure $BaFe_{12}O_{19}$ was carried out using a Physical Properties Measurement System DynaCool (Quantum Design).

III. RESULTS AND DISCUSSION

A. Evidence for chemical pressure generated by Ca^{2+} substitution

The room-temperature crystal structure of BFO is hexagonal in the space group $P6_3/mmc$ [41,42]. The unit cell of BFO can be visualized in terms of stacking of S and R blocks in the sequence RSR^*S^* [asterisk (*) marked blocks here represent in new atomic position within the block after rotating it through 180° about the hexagonal axis with respect to the new atomic in the initial block] as shown in Fig. 1(a). The S block contains two close-packed layers of oxygen, whereas the R block consists of three close-packed layers of oxygen in a hexagonal close-packed arrangement with one oxygen in the middle layer being replaced with Ba. Oxygen atoms in the hexagonal unit cell occupy $4e$, $4f$, $6h$, $12k$, $12k$ Wyckoff positions. The Ba atoms go to the Wyckoff site $2d$. Fe atoms occupy five different Wyckoff sites $2a$, $4f_2$, $12k$ (octahedral sites), $4f_1$ (tetrahedral site), and $2b$ [trigonal bipyramidal (TBP)] site as can be seen from Fig. 1(b). At room temperature, the Fe spins are ferromagnetically coupled within the "ab" plane but the spins at the $2a$, $2b$, $12k$ sites are antiparallel to those at the $4f_1$, $4f_2$ sites in the c direction. Since the number of up (16 spins) and down (8 spins) spins are unequal, $BaFe_{12}O_{19}$ shows an Ising-type collinear ferrimagneitc ordering of spins [43] with a large net magnetic moment of $20\mu_B$ per formula unit and a Curie temperature of $T_N = 720$ K. At room temperature, x-ray and neutron as well as first-principles studies have revealed that the Fe^{3+} ion does not sit at the center of the TBP (at the $2b$ site) but is displaced away from the mirror plane to the $4e$ sites along the c axis. But this off-center displacement cannot be captured on the basis of Rietveld refinements and accordingly we have placed the Fe atom in the TBP coordination at the $2b$ site [25,26,42].

Since the Ca^{2+} ion is much smaller in size than the Ba^{2+}, it is expected to generate positive chemical pressure and the unit-cell volume should accordingly decrease with increasing Ca^{2+} content (x). To confirm this, we carried out Rietveld refinement using SXRD data for various compositions of BCFO-x. The positional coordinates of the atoms in the asymmetric unit used in the refinement are 2/3,1/3,0.25 for Ba at the $2d$ site; 0,0,0 for Fe1 at the $2a$ site; 0,0,0.25 for Fe2 at the $2b$ site; 1/3,2/3,z for Fe3 at the $4f1$ site; 1/3,2/3,z for Fe4 at the $4f2$ site; x,y,z for Fe5 at the $12k$ site; 0,0,z for O1 at the $4e$ site; 1/3,2/3,z for O2 at the $4f$ site; x,y,0.25 for O3 at the $6h$ site; x,y,z for O4 at the $12k$ site; and x,y,z for O5 at the $12k$ site. Table I lists the refined structural parameters for all the compositions. We have obtained excellent fits between the observed and calculated profiles after Rietveld refinement for all the compositions. This is illustrated in Fig. 2 for $x = 0$ (i.e., BFO) and $x = 0.10$. Our Rietveld refinements confirm

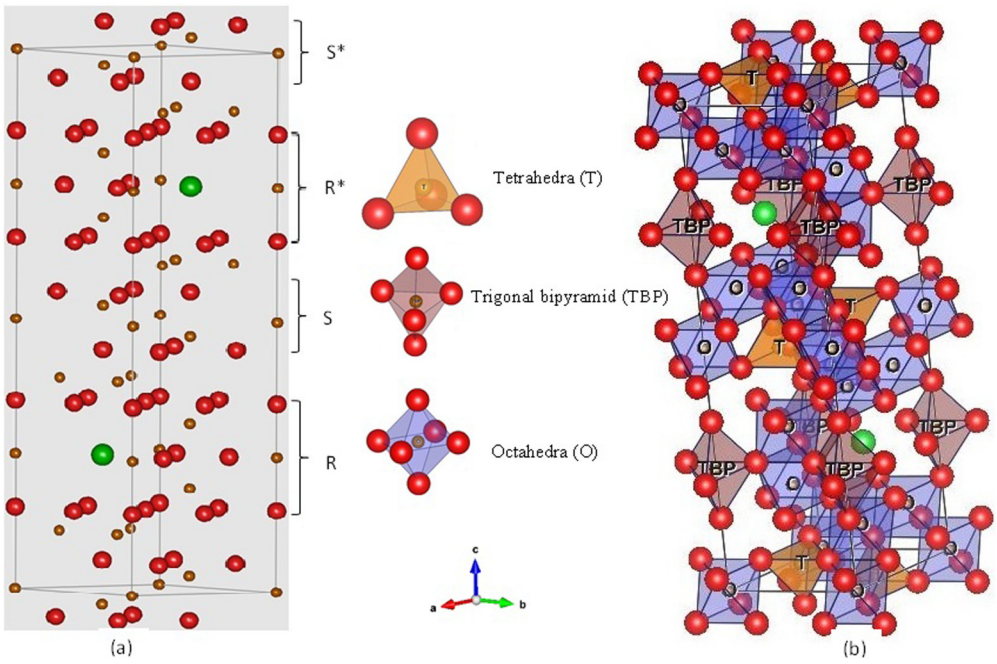

FIG. 1. (a) Unit cell and (b) coordination polyhedra of M-type hexaferrites.

that the structure of BCFO-x ($x > 0$) remains identical to BFO ($x = 0$), i.e., hexagonal in the $P6_3/mmc$ space group.

Figures 3(a) and 3(b) depict the variation of lattice parameters (a,c) and unit-cell volume (V) as a function of Ca^{2+} content (x), respectively. The fact that the unit-cell volume decreases with increasing "x" confirms that Ca^{2+} substitution generates positive chemical pressure in the BFO matrix. In addition to generating chemical pressure, Ca^{2+} substitution may also lead to creation of local electric dipoles because the smaller ions like Ca^{2+} have a tendency to go off-center with respect to the Ba^{2+} site in the center of the AO_{12} polyhedra, as is well known for Ca^{2+}-doped $SrTiO_3$ (SCT) [16,44] or Li^{1+}-doped $KTaO_3$ (KTL) systems [19,45,46]. We also calculated the bond lengths in the ab plane (Fe2-O3) and along the c axis (Fe2-O1) using FULLPROF SUITE [40] from the refined positional coordinates. Figure 3(c) depicts their variation with x. As expected, these bond lengths also decrease with increasing Ca^{2+} content. The refined structural parameters and bond lengths for all the compositions are listed in Table I.

B. Effect of Ca^{2+} substitution on quantum critical behavior of BFO

To understand the effect of chemical pressure and local electric field due to off-centered Ca^{2+} ions on the quantum critical behavior of BFO, we show in Fig. 4 the temperature dependence of the real $\varepsilon'(T)$ and imaginary $\varepsilon''(T)$ parts of the dielectric permittivity of BCFO-x in the temperature range 1.66–100 K measured at 300 kHz. It is evident from Fig. 4(a) that pure BFO shows a smeared dielectric response with a critical temperature $T_c \sim 2.91$ K which is in excellent agreement with the theoretical predictions of a transition at $T_c \sim 3$ K [26]. Ca^{2+} substitution enhances T_c and also makes the dielectric anomaly more prominent by increasing the peak height at the critical temperature. The increase in T_c seems to be primarily due to an increase in the strength of the dipole-dipole interactions both in the ab plane as well as along the c axis as a result of the contraction of the bond lengths of the FeO_5 TBPs caused by chemical pressure generated by Ca^{2+} [see Fig. 3(c)]. This is consistent with the theoretical predictions also according to which external compressive stresses should in general enhance T_c [26]. The T_c in other doped quantum paraelectric systems, such as SCT [16] and KTN [19,46], is known to follow $(x-x_c)^{1/2}$-type composition dependence in the quantum critical regime [16,38,39,46] in marked contrast to $(x-x_c)$-type dependence for the classical phase transitions [39,46]. The variation of T_c of BCFO-x as a function of Ca^{2+} content (x) also follows $(x-x_c)^{1/2}$-type dependence as can be seen from Fig. 5. The continuous line in this figure through the data points is the least-squares fit to $(x-x_c)^{1/2}$-type dependence of T_c. Interestingly, the extrapolation of the $T_c \sim (x-x_c)^{1/2}$ plot for BCFO-x to $x = 0$ gives a value of $T_c \sim 2.85$ K for undoped BFO in perfect agreement with the experimentally observed peak temperature $T_c = 2.91$ K shown in the inset of Fig. 4(a) and the theoretically predicted $T_c \sim 3$ K [26]. Further, T_c approaches 0 K on the negative side of the composition axis suggesting that negative pressure is required to locate the QCP of BFO. This is similar to the situation reported in some heavy fermion systems undergoing quantum phase transitions where QCP lies on the negative pressure axis of the phase diagram [10,47]. Such a negative pressure in BFO can be generated by substitution with a larger isovalent ion such as Pb^{2+} and we predict that Pb^{2+} substitution can drive BFO closer to its QCP in contrast to Ca^{2+} which drives it away from the QCP. Our results thus reveal that BFO is very close to QCP, but its true QCP can be realized by applying negative pressure. Before we close this discussion, we

TABLE I. Atomic positions obtained from the Rietveld refinement for different compositions.

Atoms	$x = 0.00$	$x = 0.05$	$x = 0.07$	$x = 0.10$
a (Å)	5.9723(2)	5.9707(4)	5.9700(5)	5.9690(3)
c (Å)	23.540(2)	23.521(3)	23.509(3)	23.501(2)
B(Ba/Ca)	0.5(2)	0.1(1)	0.2(2)	0.3(2)
B(Fe1)	0.3(4)	0.2(5)	0.4(5)	0.4(6)
B(Fe2)	1.1(4)	1.1(6)	1.1(5)	1.4(7)
Z_{Fe3}	0.0272(6)	0.0273(8)	0.0272(7)	0.0272(7)
B(Fe3)	0.3(3)	0.1(3)	0.2(3)	0.3(4)
Z_{Fe4}	0.1904(5)	0.1904(7)	0.1904(7)	0.1904(8)
B(Fe4)	0.4(2)	0.3(3)	0.4(3)	0.4(4)
X_{Fe5}	0.168(2)	0.168(3)	0.168(3)	0.168(3)
Y_{Fe5}	0.337(4)	0.337(6)	0.337(5)	0.337(6)
Z_{Fe5}	−0.1082(3)	−0.1083(4)	−0.1083(4)	−0.1084(4)
B(Fe5)	0.5(1)	0.4(1)	0.4(2)	0.4(1)
Z_{O1}	0.151(2)	0.151(3)	0.151(2)	0.151(3)
B(O1)	0.4(1)	0.0(2)	0.3(2)	0.4(2)
Z_{O2}	−0.054(2)	−0.054(3)	−0.054(2)	−0.054(3)
B(O2)	0.2(1)	0.2(2)	0.1(2)	0.1(2)
X_{O3}	0.18(1)	0.18(1)	0.181(1)	0.180(1)
Y_{O3}	0.36(2)	0.36(3)	0.36(2)	0.361(3)
B(O3)	0.2(9)	0.1(1)	0.2(1)	0.4(1)
X_{O4}	0.156(7)	0.157(9)	0.157(9)	0.15(1)
Y_{O4}	0.31(1)	0.31(2)	0.31(2)	0.31(2)
Z_{O4}	0.051(1)	0.052(1)	0.052(1)	0.052(2)
B(O4)	0.4(6)	0.1(8)	0.2(7)	0.3(8)
X_{O5}	0.501(9)	0.50(1)	0.500(9)	0.50(1)
Y_{O5}	1.00(2)	1.00(2)	1.00(2)	1.00(2)
Z_{O5}	0.149(1)	0.149(2)	0.149(2)	0.149(2)
B(O5)	0.5(6)	0.03(9)	0.3(8)	0.034(7)
χ^2	1.13	1.12	1.47	0.785
R_{wp}	3.15	3.90	4.06	4.19
R_{exp}	2.97	3.68	3.79	4.73
Fe2-O1	2.326(5)	2.317(7)	2.315(7)	2.310(7)
Fe2-O3	1.874(5)	1.872(7)	1.871(6)	1.870(7)

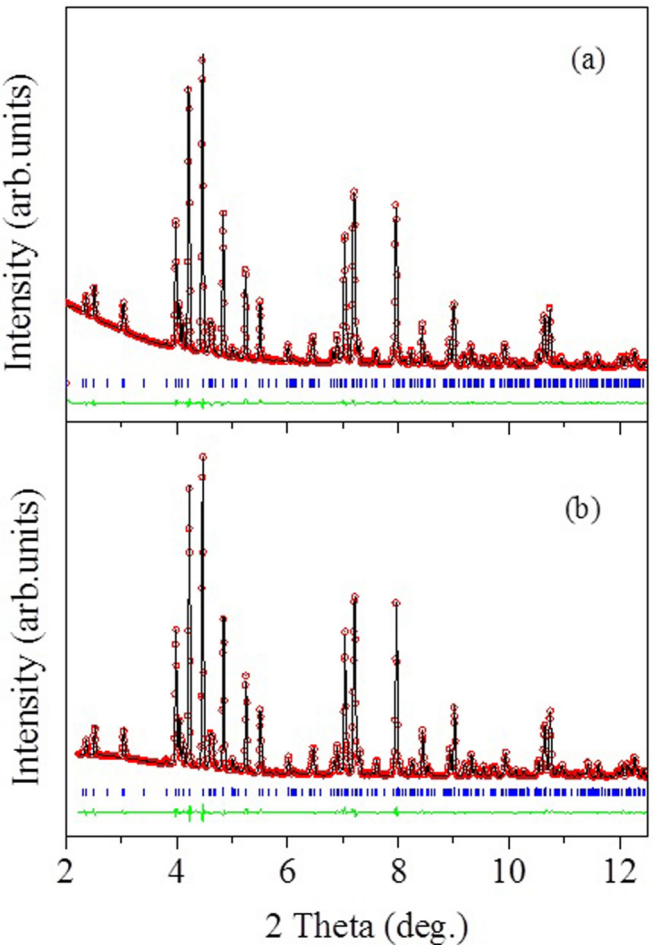

FIG. 2. (a) Observed (red circles), calculated (black continuous line), and difference (bottom green line) profiles obtained after Rietveld refinement using $P6_3/mmc$ space group for $Ba_{(1-x)}Ca_xFe_{12}O_{19}$ with (a) $x = 0.00$ and (b) $x = 0.10$. The vertical bars represent the Bragg peak positions (blue).

would like to add that BCFO-x compositions exhibit another transition around 20 K seen in Fig. 4 linked with a magnetic phase transition which is the subject matter of a separate publication.

C. Evidence for quantum electric dipole glass state in Ca^{2+} substituted BFO

The positive chemical pressure and/or local electric field generated by random site dipoles associated with off-centered cations are known to suppress quantum fluctuations [39] and stabilize quantum ferroelectric/ferrielectric phases in SCT [16,44], quantum ferroelectric state in $KTaO_3$: Nb (KTN) [39] and quantum dipole glass state in KTL [45]. Unlike the SCT, KTN and KTL systems, the geometrical frustration in Ca^{2+}-doped BFO (e.g., BCFO-x) may lead to three different types of phases below the dielectric peak temperature T_c: (1) a long range order (LRO) state as observed in SCT [16,44] and predicted for BFO also as in Ref. [26], (2) a quantum dipole glass state with a characteristic critical dynamics showing ergodicity breaking similar to KTL [45], and (3) QEDL state as proposed in Ref. [27] for BFO. The $\varepsilon'(\omega,T)$ plots near the peak temperature T_c, measured at several frequencies (in the 40–400 kHz range) at a very slow heating rate of 0.1 K/min, reveal considerable dispersion for all the compositions (see the insets of Fig. 4). Further, the temperature T'_m corresponding to the peak in $\varepsilon'(\omega,T)$ for $x \geqslant 0.03$ shifts to higher temperatures on increasing the measuring frequencies ($\omega = 2\pi f$). Figures 6(a) and 6(b) depict the $\varepsilon'(\omega,T)$ plots for a wider frequency range for $x = 0$ and $x = 0.05$, respectively, on a magnified scale for better clarity. It is evident from these figures that the dielectric peak temperature shifts to higher frequencies for the doped samples only as no such shift is observed for the undoped BFO down to 500 Hz. However, even undoped BFO shows considerable dispersion in the value of ε' indicating highly degenerate ground state with possible low-temperature tunneling among the various states. Frequency-dependent shift of the dielectric peak temperature is known to occur in glassy systems [19,45]. The nonlinear nature of the $\ln(\tau)$ versus $1/T$ plot shown in Fig. 7 for $x = 0.05$ rules out Arrhenius behavior of the relaxation time τ. A similar situation holds well for $x = 0.07$ and 0.10 also. We could model the temperature dependence of τ of all the compositions

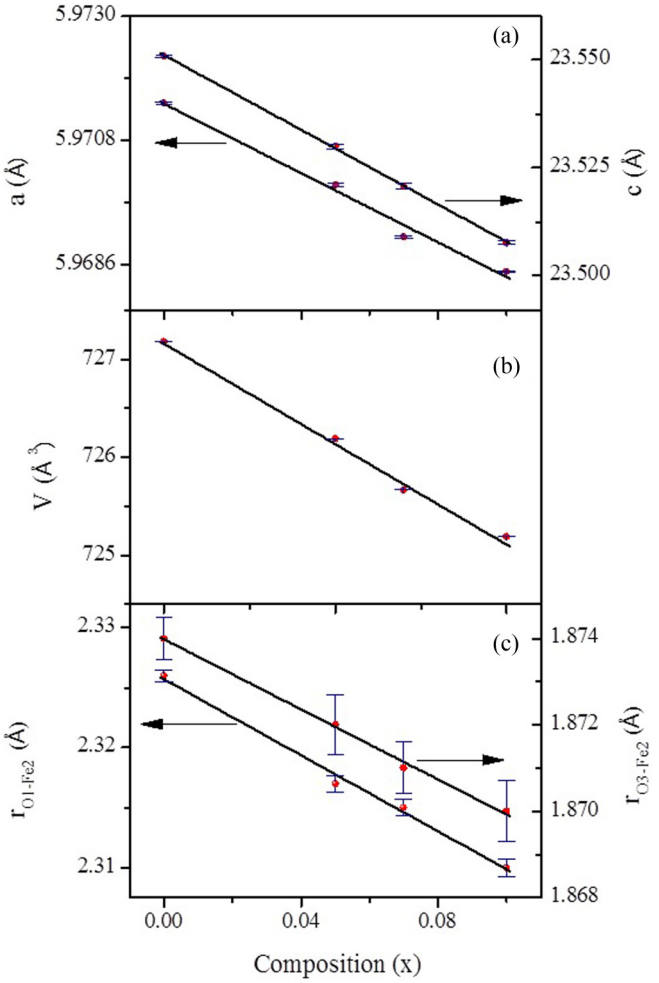

FIG. 3. Variation of (a) lattice parameters a,c, (b) unit-cell volume V, and (c) bond lengths Fe2-O1 and Fe2-O3 of $Ba_{(1-x)}Ca_xFe_{12}O_{19}$ in the composition range $0.00 \leqslant x \geqslant 0.10$.

for $x > 0.03$ using power-law dynamics, commonly used in spin-glass systems [48]:

$$\tau = \tau_0 \left(\frac{T_{\max} - T_g}{T_g} \right)^{-z\nu}, \tag{1}$$

where $\tau_0 = 1/\omega$ is the inverse of the attempt frequency, T_g the critical temperatures at which the slowest polar dynamics diverges signaling ergodicity breaking, z the dynamical critical exponent for the correlation length, and ν the critical exponent related to the correlation length. The fit corresponding to the power-law behavior is shown in the inset of Fig. 7 for $x = 0.05$. The critical exponent increases from $z\nu = 0.94 \pm 0.002$ K to 1.89 ± 0.004 K on increasing Ca^{2+} content from $x = 0.05$ to 0.10 but remains within the limit of canonical glasses as discussed in the context of the spin-glass systems [48]. Similarly, the attempt frequency also increases from 9.9×10^6 to 1.08×10^8 with Ca^{2+} content. Our analysis clearly shows that Ca^{2+} substitution induces a crossover from diffuse transition behavior in BFO with $T_c \sim 2.91$ K, as evidenced by the smeared $\varepsilon'(T)$ response for $x = 0$ with absence of frequency-dependent shift of T_c, to a canonical quantum dipole glass phase with dielectric peak temperature shifting to the higher-temperature side with increasing frequency of ac drive field. We find that the glass freezing temperature T_g also shows $(x-x_c)^{1/2}$-type composition dependence (see inset of Fig. 5) with a better fit as compared to that for T_c at 300 kHz shown in the main figure.

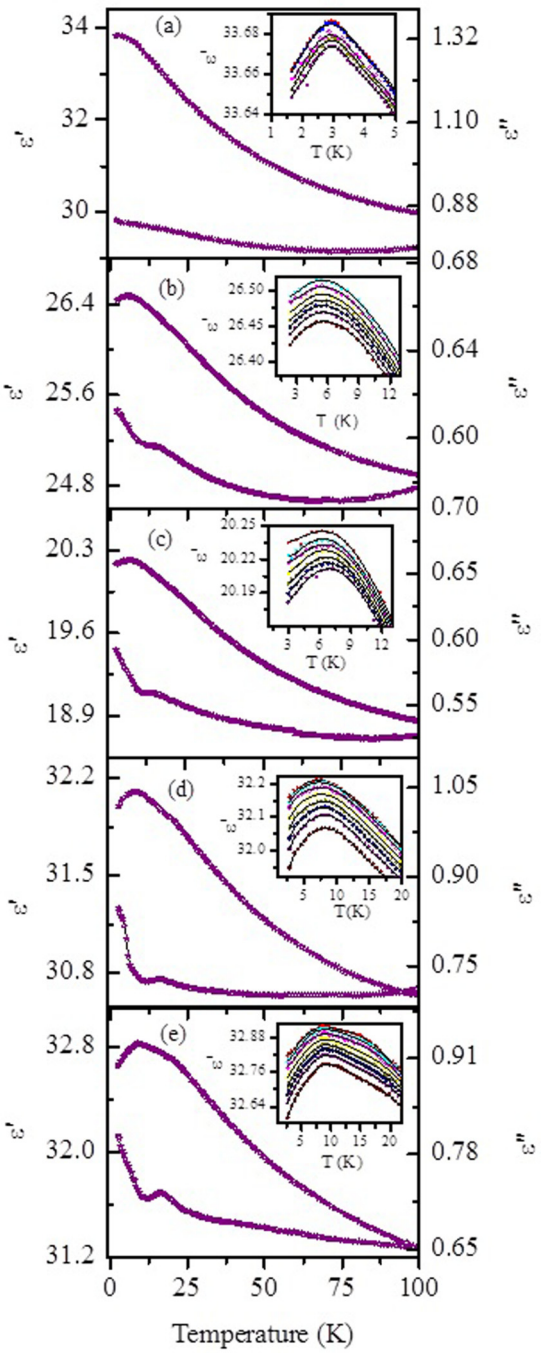

FIG. 4. Variation of the real (ε') and imaginary (ε'') parts of the dielectric permittivity of $Ba_{(1-x)}Ca_xFe_{12}O_{19}$ at 300 kHz for different Ca^{2+} concentrations with x = (a) 0.00, (b) 0.03, (c) 0.05, (d) 0.07, and (e) 0.10. Insets show the variation of the real part of the dielectric permittivity at various frequencies [40 kHz (□), 50 kHz (•), 70 kHz (△), 80 kHz (▼), 100 kHz (◇), 150 kHz (◀), 200 kHz (▷), 250 kHz (⬢), 300 kHz (☆), and 400 kHz (⬟)].

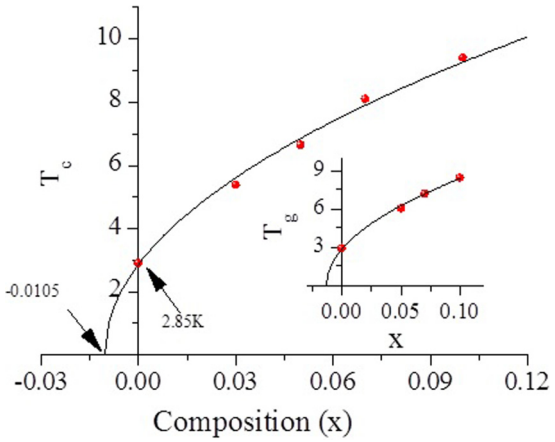

FIG. 5. Variation of dielectric peak temperature (T_c) at 300 kHz of $Ba_{(1-x)}Ca_xFe_{12}O_{19}$ as a function of Ca^{2+} concentration (x). Inset shows variation of glass transition temperature (T_g) as a function of Ca^{2+} concentration (x).

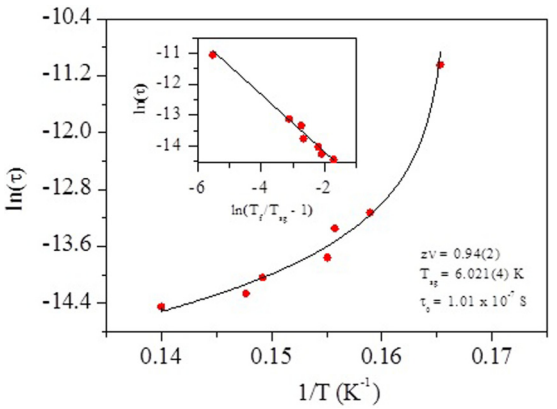

FIG. 7. Non-Arrhenius behavior of temperature dependence of relaxation time (τ) shown in $\ln\tau$ versus $1/T$ plot of $Ba_{(1-x)}Ca_xFe_{12}O_{19}$ for $x = 0.05$. The continuous line shows fit for the power-law dynamics $\tau = \tau_0(\frac{T_{max}-T_g}{T_g})^{-z\nu}$ characteristic of a dipolar glass transition. The inset shows fit for $\ln\tau$ vs $\ln(\frac{T_{max}-T_g}{T_g})$ plot.

D. Evidence for QEDL phase

The dielectric permittivity of BFO is anisotropic with a value of $\varepsilon_c \sim 42$ and $\varepsilon_{ab} \sim 18.2$ along the c axis and the ab plane, respectively [24]. The QPE behavior (i.e., increase in the dielectric permittivity followed by its approximate saturation below $\sim$10 K) is shown by ε_c only due to softening of the transverse optical phonon mode of A_{2u} symmetry [26,49] imparting to BFO a uniaxial character with dipoles aligned along the c axis. The value of dielectric permittivity of BFO in our case is $\sim$33.67 at $\sim$3 K which in effect corresponds to an average over a large number of randomly oriented polycrystalline grains each with $\varepsilon_c \sim 42$ and $\varepsilon_{ab} \sim 18.2$. The ε_c of BFO increases with decreasing temperature and was reported to saturate below $\sim$10 K, whereas the ε_{ab} decreases and saturates to a nearly constant value for $T < 50$ K [24]. This suggests that the temperature dependence of dielectric permittivity $\varepsilon\,(T)$ of sintered polycrystalline BFO below 50 K would be essentially due to the temperature dependence of ε_c only and we can analyze the data to examine the critical exponents of undoped and doped BFO in the low-temperature range up to 50 K. The Curie-Weiss temperature T_{CW}, obtained from the extrapolation of the linear region in Curie-Weiss plots up to $\sim$40 K (see Fig. 8) is found to be negative for all the compositions in the range $0 \leqslant x \leqslant 0.1$ as expected for AFE correlations. The magnitude of T_{CW} increases with increasing Ca^{2+} content (see Fig. 9). Since T_c of BFO is $\sim$2.91 K, whereas $|T_{CW}|$ is $\sim$423 K, the frustration parameter $f = |T_{CW}|/T_c$ is very high ($\sim$141) and lies in the range where quantum spin liquid phase has been reported in the magnetic systems [2,50].

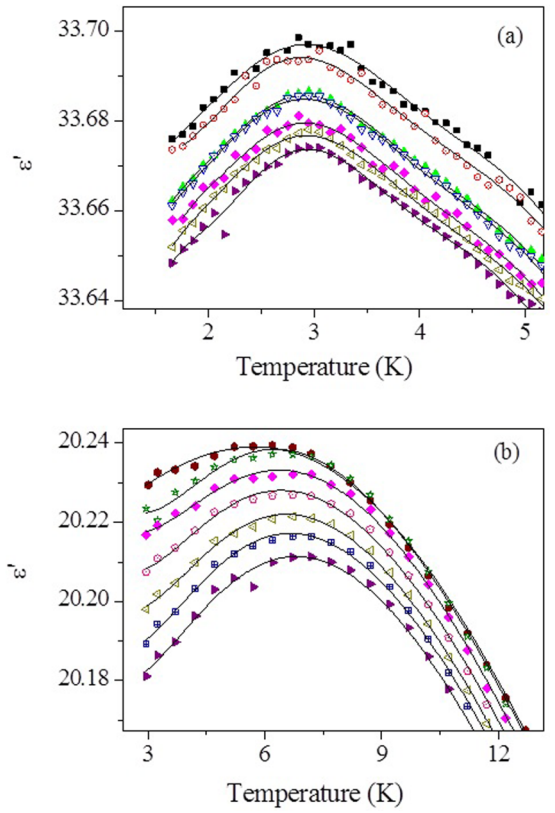

FIG. 6. Variation of the real (ε') part of the dielectric permittivity of $Ba_{(1-x)}Ca_xFe_{12}O_{19}$ for (a) $x = 0$ and (b) $x = 0.05$ measured at various frequencies [500 Hz (■), 1 kHz (◯), 10 kHz (⬢), 50 kHz (▲), 70 kHz (▽), 80 kHz (☆), 100 kHz (⧫), 150 kHz (□), 200 kHz (◁), 250 kHz (⊞), and 300 kHz (▶)].

One of the criteria used to define a quantum spin liquid (QSL) phase in magnetic systems is linear temperature dependence of specific heat at low temperatures [2,36,51,52]. The temperature dependence of the specific heat of BFO from 1.8 to 300 K is shown in Fig. 10. The specific-heat plot does not reveal any sharp anomaly around $T_c = 2.91$ K, expected for a phase transition to a LRO AFE phase or glassy freezing, as can be seen more clearly from the inset (a) of Fig. 10 on a magnified scale. On the contrary, it shows linear temperature dependence in the 1.8 to 2.5 K temperature range below T_c with a knee around 3.5 K. Such a linear temperature dependence of specific heat points toward the QEDL state in close analogy with the QSL state [2,36,51,52]. Even after application of magnetic fields up to 6 T, we did not see any

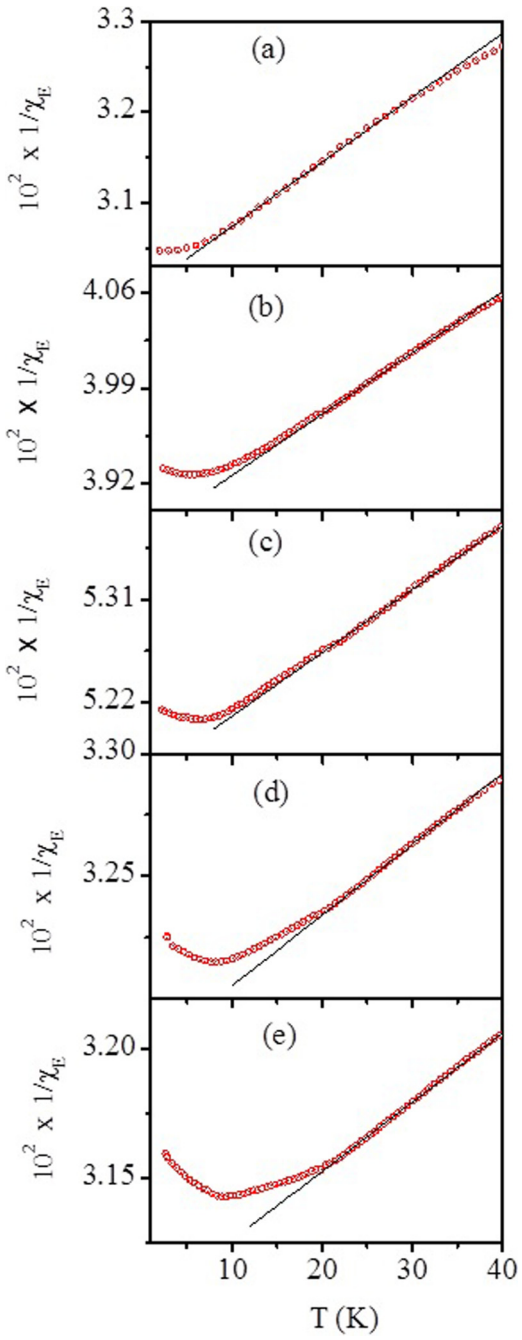

FIG. 8. Curie-Weiss fit (black solid line) to temperature-dependent permittivity (red circles) of $Ba_{(1-x)}Ca_xFe_{12}O_{19}$ for $x =$ (a) 0.00, (b) 0.03, (c) 0.05, (d) 0.70, and (e) 0.10.

departure from the linear behavior suggesting that this feature is linked with electric dipoles only and not the magnetic spins of the lattice. The signature of the QEDL state is better seen after subtracting the Debye lattice contribution at low temperatures (T^3 dependence) in this nonmetallic system. Since the underlying magnetic sublattice is predominantly ferrimagnetic with large magnetic moment, one expects a $T^{3/2}$ dependence for the magnetic LRO phase [53]. Taking both aspects together, the specific heat of BFO should exhibit $C_p = \alpha T^3 + \beta T^{3/2}$ type temperature dependence at very low temperatures. This was confirmed by the linearity of the

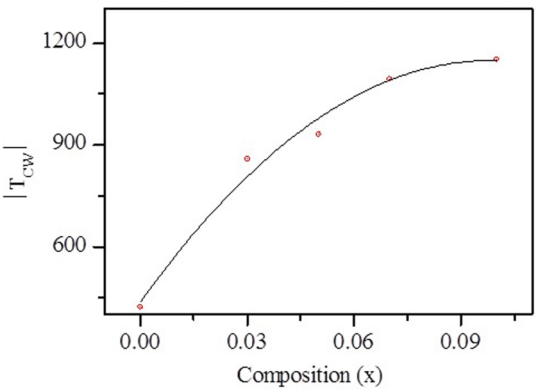

FIG. 9. Variation of the magnitude of Curie-Weiss temperature $|T_{CW}|$ of $Ba_{(1-x)}Ca_xFe_{12}O_{19}$ with concentration (x).

$C_p/T^{3/2}$ vs $T^{3/2}$ plot shown in inset (b) of Fig. 10 in the temperature range 1.8–11.8 K. Using this fit, we subtracted the Debye contribution to obtain the non-Debye part which is shown in inset (c) of Fig. 10. The non-Debye part of specific heat also shows a linear temperature dependence below the dielectric anomaly peak temperature $T_c \sim 2.91$ K of undoped BFO. The positive curvature at low temperatures may be due to the nonzero entropy in the ground-state characteristic of a geometrically frustrated system [2,35,52]. The linear temperature dependence of the non-Debye part of the specific heat below ~3 K is not of magnetic origin as it does not show any field dependence up to 6T [see inset (c) of Fig. 10]. Magnetic field leads to a slight decrease in the specific heat above 3 K and transforms the steplike feature of non-Debye contribution of zero-field measurement to a broad peak [see inset (c) of Fig. 10]. The linear temperature dependence of specific heat and its field independence points toward a QEDL state below 3 K, although more work is required at much lower temperatures than those used in

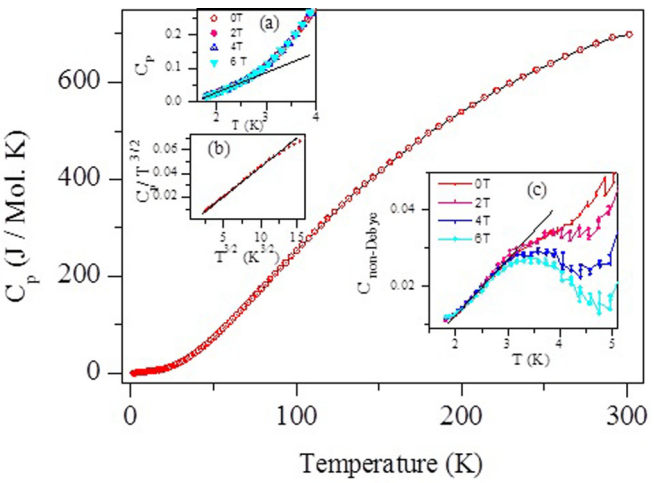

FIG. 10. Specific heat of pure $BaFe_{12}O_{19}$ as a function of temperature. Insets: (a) specific heat measured at different fields shown on a magnified scale, (b) $C_p/T^{3/2}$ vs $T^{3/2}$ plot where the solid line represents the linear fit, and (c) non-Debye part of the specific heat at different magnetic fields.

the present work to confirm this proposition. The excess specific heat of non-Debye and nonmagnetic origin clearly suggests the presence of low-energy excitations. We hope that our results would encourage inelastic neutron-scattering experiments with appropriate theoretical models to understand the precise nature of these excitations and their possible role in the QEDL state.

IV. SUMMARY

To summarize, we have shown that $BaFe_{12}O_{19}$ exhibits a smeared dielectric response due to AFE correlations peaking at $T_c \sim 2.91$ K with a frustration parameter $f \sim 141$. We have also presented results of specific-heat measurements at different magnetic fields which suggest the possibility of a quantum electric dipole liquid state in this compound below T_c. We have investigated the quantum critical behavior of $BaFe_{12}O_{19}$ by driving it away from the QCP through a nonthermal variable, namely, chemical pressure generated by Ca^{2+} substitution. Using Rietveld analysis of SXRD data, we have shown that the unit-cell volume decreases with increasing Ca^{2+} content (x) confirming positive chemical pressure generated by Ca^{2+} substitution. Our dielectric measurements reveal that the chemical pressure generated by Ca^{2+} substitution stabilizes a quantum electric dipole glass state whose glass transition temperature (T_g) follows $(x-x_c)^{1/2}$ type of composition dependence expected for a quantum phase transition. Our results reveal that $BaFe_{12}O_{19}$ is close to its QCP but not quite at it. We propose that the QCP of BFO can be reached by applying negative chemical pressure.

V. ACKNOWLEDGMENTS

D.P. acknowledges financial support from Science and Engineering Research Board (SERB) of India through the award of a J C Bose National Fellowship. The authors sincerely acknowledge Professor T. V. Ramakrishnan for fruitful discussions and reading of the manuscript. We acknowledge support from India-DESY project of the Department of Science and Technology, Government of India operated through Jawaharlal Nehru Centre for Advanced Scientific Research, Jakkur, India. We thank beamline scientist Dr. Martin Etterat PETRA III for his help in setting up the experiments.

[1] J. A. Hertz, Phys. Rev. B **14**, 1165 (1976).
[2] L. Balents, Nature (London) **464**, 199 (2010).
[3] R. B. Laughlin, Adv. Phys. **47**, 943 (1998).
[4] S. V. Kravchenko, W. E. Mason, G. E. Bowker, J. E. Furneaux, V. M. Pudalov, and M. D'Iorio, Phys. Rev. B **51**, 7038 (1995).
[5] S. Sachdev, *Quantum Phase Transitions*, 2nd ed. (Cambridge University Press, Cambridge, UK, 2011).
[6] J. Orenstein and A. J. Millis, Science **288**, 468 (2000).
[7] C. Toke, P. E. Lammert, V. H. Crespi, and J. K. Jain, Phys. Rev. B **74**, 235417 (2006).
[8] N. D. Mathur, F. M. Grosche, S. R. Julian, I. R. Walker, D. M. Freye, R. K. W. Haselwimmer, and G. G. Lonzarich, Nature (London) **394**, 39 (1998).
[9] W. Knafo, R. Settai, D. Braithwaite, S. Kurahashi, D. Aoki, and J. Flouquet, Phys. Rev. B **95**, 014411 (2017).
[10] V. A. Sidorov, M. Nicklas, P. G. Pagliuso, J. L. Sarrao, Y. Bang, A. V. Balatsky, and J. D. Thompson, Phys. Rev. Lett. **89**, 157004 (2002).
[11] K. Heuser, E.-W. Scheidt, T. Schreiner, and G. R. Stewart, Phys. Rev. B **57**, R4198(R) (1998).
[12] H. Lohneysen, J. Phys.: Condens. Matter **8**, 9689 (1996).
[13] G. A. Samara, Phys. Rev. Lett. **27**, 103 (1971).
[14] D. B. McWhan, C. Vettier, R. Youngblood, and G. Shirane, Phys. Rev. B **20**, 4612 (1979).
[15] S. A. Carter, T. F. Rosenbaum, J. M. Honig, and J. Spalek, Phys. Rev. Lett. **67**, 3440 (1991).
[16] J. G. Bednorz and K. A. Muller, Phys. Rev. Lett. **52**, 2289 (1984).
[17] D. Bitko, T. F. Rosenbaum, and G. Aeppli, Phys. Rev. Lett. **77**, 940 (1996).
[18] K. A. Müller and H. Burkard, Phys. Rev. B **19**, 3593 (1979).
[19] U. T. Hochli, K. Knorr, and A. Loidl, Adv. Phys. **39**, 405 (1990).
[20] I. S. Kim, M. Itoh, and T. Nakamura, J. Solid State Chem. **101**, 77 (1992).
[21] G. A. Samara and P. S. Peercy, Phys. Rev. B **7**, 1131 (1973).
[22] T. Katsufuji and H. Takagi, Phys. Rev. B **64**, 054415 (2001).
[23] U. Bianchi, J. Dec, W. Kleemann, and J. G. Bednorz, Phys. Rev. B **51**, 8737 (1995).
[24] S.-P. Shen, Y.-S. Chai, J.-Z. Cong, P.-J. Sun, J. Lu, L.-Q. Yan, S. G. Wang, and Y. Sun, Phys. Rev. B **90**, 180404(R) (2014).
[25] H. B. Cao, Z. Y. Zhao, M. Lee, E. S. Choi, M. A. McGuire, B. C. Sales, H. D. Zhou, J. Q. Yan, and D. G. Mandrus, APL Mater. **3**, 062512 (2015).
[26] P. S. Wang and H. J. Xiang, Phys. Rev. X **4**, 011035 (2014).
[27] S.-P. Shen, J.-C. Wu, J.-D. Song, X.-F. Sun, Y.-F. Yang, Y.-S. Chai, D.-S. Shang, S.-G. Wang, J. F. Scott, and Y. Sun, Nat. Commun. **7**, 10569 (2016).
[28] E. Courtens, Phys. Rev. Lett. **52**, 69 (1984).
[29] R. Ranjan, D. Pandey, and N. P. Lalla, Phys. Rev. Lett. **84**, 3726 (2000).
[30] S. K. Mishra, N. Choudhury, S. L. Chaplot, P. S. R. Krishna, and R. Mittal, Phys. Rev. B **76**, 024110 (2007).
[31] B. P. Pokharel and D. Pandey, J. Appl. Phys. **88**, 5364 (2000).
[32] S. E. Rowley, Y.-S. Chai, S.-P. Shen, Y. Sun, A. T. Jones, B. E. Watts, and J. F. Scott, Sci. Rep. **6**, 25724 (2016).
[33] M. Vojta, Rep. Prog. Phys. **66**, 2069 (2006).
[34] S. Sachdev, Science **288**, 475 (2000).
[35] A. P. Ramirez, A. Hayashi, R. J. Cava, R. Siddharthan, and B. S. Shastry, Nature (London) **399**, 333 (1999).
[36] H. D. Zhou, E. S. Choi, G. Li, L. Balicas, C. R. Wiebe, Y. Qiu, J. R. D. Copley, and J. S. Gardner, Phys. Rev. Lett. **106**, 147204 (2011).
[37] E. Matsushita and S. Segawa, Ferroelectrics **347**, 1 (2007).
[38] R. Morf, T. Schneider, and E. Stoll, Phys. Rev. B **16**, 462 (1977).
[39] U. T. Höchli, Ferroelectrics **35**, 17 (1981).
[40] J. Rodríguez-Carvajal, Laboratory, FULLPROF 2017, Laboratorie Leon Brillouin, CEA-CNRS, France, http://www.ill.eu/sites/fullprof.

[41] W. D. Townes, J. H. Fang, and A. J. Perrotta, Z. Kristallogr. **125**, 437 (1967).
[42] X. Obradors, A. Collomb, M. Pernet, D. Samaras, and J. C. Joubert, J. Solid State Chem. **56**, 171 (1985).
[43] E. W. Gorter, Proc. of IEE - Part B Radio and Electron. Eng. **104**, 255 (1957).
[44] S. K. Mishra and D. Pandey, Appl. Phys. Lett. **95**, 232910 (2009).
[45] B. E. Vugmeister and M. D. Glinchuk, Rev. Mod. Phys. **62**, 993 (1990).
[46] U. T. Hochli and L. A. Boatner, Phys. Rev. B **20**, 266 (1979).
[47] S. Friedemann, T. Westerkamp, M. Brando, N. Oeschler, S. Wirth, P. Gegenwart, C. Krellner, C. Geibel, and F. Steglich, Nat. Phys. **5**, 465 (2009).
[48] J. A. Mydosh, *Spin Glasses: An Experimental Introduction* (Taylor & Francis, London, 1993).
[49] A. S. Mikheykin, E. S. Zhukova, V. I. Torgashev, A. G. Razumnaya, Y. I. Yuzyuk, B. P. Gorshunov, A. S. Prokhorov, A. E. Sashin, A. A. Bush, and M. Dressel, Eur. Phys. J. B **87**, 232 (2014).
[50] A. P. Ramirez, Annu. Rev. Mater. Sci. **24**, 453 (1994).
[51] S. Yamashita, Y. Nakazawa, M. Oguni, Y. Oshima, H. Nojiri, Y. Shimizu, K. Miyagawa, and K. Kanoda, Nat. Phys. **4**, 459 (2008).
[52] S. Yamashita, T. Yamamoto, Y. Nakazawa, M. Tamura, and R. Kato, Nat. Commun. **2**, 275 (2011).
[53] W. N. Lawless, Phys. Rev. Lett. **36**, 478 (1976).